T. Teumer, M. Rädle and F.-J. Methner

Possibility of monitoring beer haze with static light scattering, a theoretical background

In the process engineering sub-steps of beer production, turbidity formation occurs during the brewing process. There may be several reasons for this, such as the precipitation of dissolved substances during the brewing process. However, it can also be caused by equipment malfunctions, for example malfunctions in filtration. This review examines what types of turbidity are present in beer, their origins and how they are currently measured. In order to better understand the process of turbidity, the physical meaning of turbidity will be highlighted. For this purpose, the scattering behaviour of a light beam hitting a particle will be explained. This is supplemented by a presentation of common measuring methods of such disperse-phase systems, which show how the particle size or particle size distribution can be determined and, if possible, also how to provide information about the particle composition. The focus is on static scatter measurement methods.

Descriptors: Beer, haze, static light scattering, optical measurement

1 Introduction

As early as 1898, the brewing industry began to think about what a "brilliant beer" was. Thought was given to how a beer could always be produced in the same way and how it would remain clear. This approach has not changed until today. Various working groups have compiled the different turbidity substances [4, 68, 69]. In a retrospect, various causes of turbidity are listed, both biological and non-biological, which lead to instability in the beer. It also gives a general overview of the possible sources of turbidity in beer. In order to better understand the turbidity causing particles and their possible origin, it is necessary to know the composition of beer or beer extract. Beer with an original wort content of 12% consists of 4–4.5% extract, 3.8–4.2% alcohol, 0.42–0.55% carbonic acid and 90–92% water. The average composition of the beer extract includes 80–85% carbohydrates, 4.5–5.2% protein, 3–5% glycerine, 3–4% minerals, 2–3% bitter, tanning and colouring agents, 0.7–1% organic acids and small amounts of vitamins [18, 50]. Proteins, polyphenols and carbohydrates are listed as the most frequent causes of turbidity [6, 15, 30, 50, 67–69]. Other substances can also manifest as turbidity, such as metals [3, 23, 30, 49], so-called bits which are precipitates through interactions between isinglass fining material and foam stabilizer materials [4, 68], filter auxiliary materials [4, 30, 50], living and dead microbes [4, 26, 52] and oxalates [4, 50, 68]. A further classification differentiates chill haze and permanent turbidity [4, 30, 50, 83].

https://doi.org/10.23763/BrSc19-15teumer

Authors

Tobias Teumer, Matthias Rädle, CeMOS – Center for Mass Spectrometry and Optical Spectroscopy, Mannheim University of Applied Sciences, Germany; Frank-Jürgen Methner, Chair of Brewing Science, Institute of Food Technology and Food Chemistry, Technische Universität Berlin, Germany; corresponding author: t.teumer@hs-mannheim.de

1.1 Colloidal Dispersions (Turbidity)

The word colloid derives from the Greek word "kolla" which means glue. The term dispersion is characterized as a two-phase system with finely divided solids in a liquid [76]. We speak of a colloid if one of its spatial dimensions is smaller than 1 mm. The lower limit is at about 1 nm, below which one speaks of real solutions (IUPAC definition) [21, 82]. In colloidal dispersions, the surface properties dominate the solid state properties [21]. The particles first present as molecules in the dispersion medium are subject to movement. When these particles collide, they grow into colloids, which leads to an increase in the degree of dispersion. The particle growth is influenced by Brownian motion [21, 50]. The brewing water, the clear wort or the filtered beer are the dispersing agents, the turbidifiers are the colloidal particles.

1.2 Chill Haze

Chill haze is the colloidal turbidity that occurs when the beer is cooled. It is particularly important for the brewer to know the mechanisms of chill haze since it is considered as a preliminary stage of permanent haze. Chill haze occurs when loose bonds of higher-value protein degradation products interact with highly condensed polyphenols, to which small amounts of carbohydrates and minerals are attached [30, 31]. When heated, these will dissolve again. The formation of turbidity is promoted by a decrease in temperature, the oxidation of the beer, the presence of heavy metal ions of the elements Cu and Fe, the movement of the beer and light [11, 30, 40, 83].

1.3 Permanent Haze

The chill haze changes over time into a permanent haze. This time can vary significantly depending on type of beer, the selected filling container and the storage conditions. Due to these influences, permanent haze occurs several weeks after bottling [4, 30, 31,

49, 65, 69]. The polyphenol flavan-3-ol with the protein proline as coupling partner [6, 30, 54, 55], but also α- and β-glucans [47, 50, 67] are considered to be the primary source for colloidal turbidity.

1.4 Proteins & Polyphenols (Tannins)

The reason for a large part of the organic turbidity lies in the preference of proteins to bind to polyphenols [65]. Both polymerize. The peptide proline stands out in the process [6, 65]. The turbidity is strongly dependent on the protein concentration [79]. It has been shown that beverages with a high proline and polyphenol content are more prone to turbidity than beverages containing only one of the two components [6, 51]. There are models that describe the process of precipitation and the interaction between polyphenol and the protein or specifically that of a tannin flavan-3-ol and L-proline [54–56]. Various parameters can have an influence on this behaviour, e.g. the concentration of reactants or the alcohol content. Both influence the structure of the polymeric compound [40], so that the interaction of both components can lead to turbidity.

1.5 Carbohydrates / Starch (Saccharides)

Carbohydrates can also be responsible for visible turbidity in beer. In addition to β-glucans and pentosans, beer also contains their degradation products as well as oligosaccharides, which are present in colloidal form [9, 27, 50]. The molecular weight of β-glucan can reach orders of magnitude which enabler scattering of light due to its size alone [24, 47, 67, 71].

1.6 Metals

The metals as such are not visible as pure elements. However, their ions have an oxidation catalytic effect on the beer [23, 30, 50] and their oxidation products then become visible as turbidity. They also have a precipitating effect on protein particles [49–51]. Metal ions are a part of hops and malt, and are furthermore introduced into the brewing process via the brewing water [23,30, 50].

1.7 Stabilizers and Filter Materials

Most of the inorganic particles in beer originate from stabilisation and filtration aids used to obtain a very high beer quality. [3, 8, 30, 44, 50, 59]. They can then occur in the beer as turbidity if the stabilization agents have not been sufficiently removed through filtration [50, 59, 68].

1.8 Calcium Oxalates

The oxalate turbidity is caused by the precipitation of calcium oxalate in crystalline or amorphous form [50, 68]. Oxalic acid from the malt reacts with the calcium ions from the brewing water and is then present in the beer as turbidity or as a source of germination [28, 35].

1.9 Microbes

Microorganisms that are able to grow in beer can cause turbidity. Their number is low, since the ambient conditions in the beer do not allow for a development suitable for microorganisms. These include the alcohol content, carbonic acid content, bitter substances, low pH value, anaerobic conditions, lack of carbon and nitrogen sources and low temperatures during the process. These limit the possibility of beer lactic acid bacteria, beer pediococci, gram-negative bacteria and fermenting yeasts in beer to develop [50]. If it does happen, it takes some time for the turbidity to hit [26, 50, 52].

2 Methods for the Detection of Turbidity

In the MEBAK (Methodensammlung der Mitteleuropäischen Brautechnischen Analysekommission / collection of methods of the Central European Brewing Technical Analysis Commission) you will find the methods currently used to carry out turbidity measurements in beer [42]. So far a complete compilation of the various ways of identifying the type of turbidity in beer has not been published [20, 48]. Reference is made here to a summary of methods for particle analysis and for monitoring biological and synthetic processes. This list contains all currently relevant particle analysis measurement techniques used in process monitoring [5, 33]. Identification is carried out by optical, electrical, enzymatic, microscopic or wet-chemical measuring methods. These methods usually involve considerable analytical effort.

2.1 Optical Measurement Methods

Light, neutron and X-ray scattering methods are used extensively to study the structure and dynamics of particles and macromolecules in multicomponent systems. The momentum (dipole moment) and the energy difference between the scattered light and the incident light are used to characterize the structure and dynamics of the measured material. Since scatter measurement techniques are non-destructive, they are very well suited for inline/online measurements. There are four methods primarily used for scattering measurements: Static light scattering (SLS), dynamic light scattering (DLS), turbidimetry and diffractometry, with which the turbidity can be analysed. These measurements help to determine the number, the diameter or both scales of a particle system. The measuring methods provide versatile application options. Measurements of elastic scattered light are compared with computer-aided models to determine the optically measured degree of beer turbidity [1, 16]. Different measuring angles are used for this purpose [60]. Dynamic light scattering is used for filter monitoring during beer production [29, 64]. Even highly disperse media can be monitored [70]. The turbidity perceived with the eye is thus scientifically quantified [10]. The colour of the wort is ensured through optical methods by measuring the optical density with a specific wavelength that correlates with the associated EBC value [13] which can be measured together with the turbidity, consequently the long-term stability of beer can also be improved [17]. Different optical measuring methods to measure the beer turbidity are described [48], also the possibility to combine different optical measuring techniques with each other [77]. A product-friendly measurement of the particle size is possible [74]. Dynamic light scattering methods [39] and static methods [33] can be used to predict the coloration in an emulsion [37] and the particle size. Anything that differs as refraction from its surroundings can be measured, e.g. silicone networks [2], phenols and proteins [12, 66, 73], latex particles [19, 46]. Optical

measuring methods even make it possible to identify pollen in the air [72]. Microcrystalline cellulose structures of chemically produced nanomaterials [61] are also measured with this technique. The measurement of individual particles is also carried out using optical methods [62]. For a better overview there is a summarizing comparison of the different measuring methods and different fields of application [5, 33, 75].

2.2 Coulter Counter

A coulter counter is a measuring device for measuring the number of particles in an electrically conductive liquid. It measures the change in the electric field as a particle passes a channel. With this measuring technique, individual particles can be measured and observed over a long period of time [5, 45, 75].

2.3 Gel Permeation Chromatography

In gel permeation chromatography, particles separate due to their size in a column filled with gel. This method is mainly used in the chemical industry as a tool for quality control, but is not suitable as a tool for an in/online measuring system [5, 20, 38, 57]. With this method, the sample is lost and can no longer be used. It's a destructive material testing procedure.

2.4 Gel Electrophoresis

In gel electrophoresis, the sample passes through a gel in an ionic buffer solution to which an electric field is applied. Particles move through the electric field at different speeds depending on their size and charge. This makes it easy to measure macromolecules such as proteins; however, online measurement is not possible with this method [20, 25, 63].

2.5 Enzymatic Turbidity Identification

Enzymatic turbidity identification can be used for biological particle characterization when molecules are difficult to separate from each other in the liquid phase. Accordingly specific enzymes are added to the sample [20, 47] to separate and identify the different particle species.

2.6 Microscopic Turbidity Identification

With microscopic measurement, particles in beer can be recorded and displayed as an image. This method is well suited visualize the shape of a single particle. An online approach is conceivable, but difficult to implement [20, 80].

There are other methods to characterize particles [5] such as sedimentation, centrifugation, sieving, filtration, ultrasonic measurements, field-flow fractionation, velocimetry, which are not further discussed here.

3 Static Light Scattering

The study of the scattering of light and its applications cover a very wide area. Static light scattering is used as a tool to obtain information about particle sizes. The scattering of light at colloidal dispersions is measured and evaluated within the classical theory of wave properties of light and electromagnetic waves [7]. When describing optical phenomena towards the end of the 17th century, Huygens had proposed a model to describe the propagation of light via a wave approach in analogy to the propagation of sound waves [81]. The Huygens' principle states that every point on a primary wavefront serves itself as the source of a secondary elementary wave. These waves propagate according to the composition of the medium. In a homogeneous, isotropic medium, the elementary waves are spherical waves. The foremost line of the elementary wave is thus the wavefront of light [81]. This approach says nothing about the diffractive effect of the medium itself. Fresnel was able to extend Huygens' principle. He replaced the concept of the enveloping elementary wave with a calculation rule. The Huygens-Fresnel principle states that the light field at a point P is formed by summation of the amplitude and phase of all contributions originating from the elementary waves. In his treatise Fresnel introduced a "deflection angle" as a factor, the exact form of which Kirchhoff first specified. Fresnel's description correctly reflects a variety of diffraction phenomena. The polarization-dependent reflectivity, described by Malus, as well as the discovery of the interference principle and the transversality of light waves by Young, were further pillars of wave theory [81]. Many special cases had already been described, which Maxwell summarized with four equations. Maxwell combined Ampere's law and Gauss's law with the induction law and additionally introduced the displacement current in order not to violate the continuity equation [32, 36].

The starting point for investigating the scattering of light by a particle is the study of irradiation passing through an optically transparent plate, shown in figure 1. An incident wave E_W meets a denser medium. At the plate border a part of the wave is reflected while the rest penetrates through the border surface. On the opposite side the same interaction occurs, part of the penetrating wave is reflected, the rest penetrates the second side of the plate and exits. The emerging wave is regarded as the transmitting part of the wave. The incident wave E_W is treated the same for both the plate and the particle. What is described for the plate as reflection and transmission is summarized as scattering

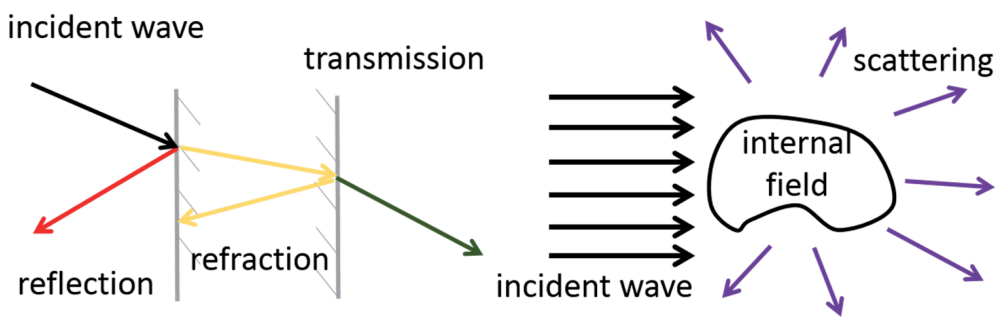

Fig. 1 Analogy between incident light on a plate and a particle

wave E_S for the particle. What is the refraction for the plate is considered an internal field for the particle. Thus, in analogy to the equations for the plate, Maxwell's equations can be established which describe the scattering at the particle. In order to make the observation as simple as possible, the resulting electric field E_S and magnetic field H_S are broken down into their Fourier components, which are plane waves. The absorption scattering problem can be solved by superposition independently of the illumination of the particles. The field inside the particle is described with (E_1, H_1). The field (E_2, H_2) of the surrounding medium is the superposition of the incident field (E_W, H_W) and the scattering field (E_S, H_S), as described in equation 1 [7].

$$E_2 = E_W + E_S \; ; \; H_2 = H_W + H_S$$

$$E_W = E_0 e^{(i\omega t - ikx)} \; ; \; H = H_0 e^{(i\omega t - ikx)} \qquad \text{(Eq. 1)}$$

The wave factor k corresponds to the surrounding medium, with the angular frequency ω which is defined temporally by t and spatially by x. The imaginary part of the wave is taken into consideration by the term i. Maxwell's equations must be fulfilled at all points where the field constant ε and the permeability μ are constant. Any vector field that has no deviation and satisfies the vector wave equation can be considered an electric field. At the transition of the phase boundary between particle and medium there is a change of properties and thus also for ε and μ. The following boundary conditions apply at such a transition point,

$$[E_2(x) - E_1(x)] \times \acute{n} = 0; x \; on \; A$$

$$[H_2(x) - H_1(x)] \times \acute{n} = 0; x \; on \; A \qquad \text{(Eq. 2)}$$

where $\acute{n}$ is the outward-pointing normal perpendicular to the outer surface A of the particle. These boundary conditions are the prerequisites for the tangential components E and H to be continuous across the boundaries. Equation 2 is the condition for the superposition of all points distributed over the boundary surface. It is necessary to assume plane, monochromatic waves. A random polarization can be seen as a superposition of two orthogonal polarization states. With this assumption, each scattering problem has to be solved only twice in order to determine the random scattering with a random polarization with a given wave propagation. At this point Stokes parameters are introduced, as shown in equation 3. This description of the states is more than a mathematical tool, it can be used to make polarizers that can let one of the components described here pass and filter the others [7].

$$I = E_\parallel E_\parallel{}^* + E_\perp E_\perp{}^* = a_\parallel{}^2 + a_\perp{}^2$$
$$Q = E_\parallel E_\parallel{}^* - E_\perp E_\perp{}^* = a_\parallel{}^2 - a_\perp{}^2$$
$$U = E_\parallel E_\perp{}^* + E_\perp E_\parallel{}^* = 2a_\parallel a_\perp \cos\delta$$
$$V = i(E_\parallel E_\perp{}^* - E_\perp E_\parallel{}^*) = 2a_\parallel a_\perp \sin\delta \qquad \text{(Eq. 3)}$$

The irradiance I often casually also called light intensity corresponds to the intensity without a polarizer, the parameters Q,U,V represent different settings with polarizers and the total transmissive radiation depending on these settings. $E_{\parallel,\perp}$ stands for the luminous intensity of the parallel and perpendicular polarization in front of the polarizer, $E_{\parallel,\perp}{}^*$ correspondingly after the polarizer. The phase δ is the difference between the two polarization directions. The Stokes parameters can be used to describe the processes involved in the scattering of a monochrome wave on a particle, as illustrated in figure 2 [7]. The direction of propagation of the incoming electromagnetic wave is in the direction of the positive z-axis, also called the forward direction selected as the 0-point of the Cartesian coordinate system. Any point in the particle may be selected as the 0-point of the Cartesian coordinate system. The x-axis and the y-axis are orthogonal to the z-axis and to each other but otherwise randomly aligned. For each direction an orthonormal vector $\acute{e}_x$, $\acute{e}_y$, $\acute{e}_z$ in the respective positive directions of the axes x, y, z is applied to these. The scattering plane is defined by the scattering direction $\acute{e}_r$ and the forward direction $\acute{e}_z$. The scattering plane is clearly determined by the azimuth angle ϕ except when $\acute{e}_r$ runs parallel to the z-axis. In its two states $\acute{e}_r = \pm \acute{e}_z$, each plane containing the z-axis is a suitable scattering plane. It is practical to decompose the incident electromagnetic field E_W, which lies in the y, x plane, into its parallel and perpendicular components. This case is based on the solution of Maxwell's equation for an electromagnetic wave, adapted with the polarization data of the electric fields of the electromagnetic wave, written with its unit vectors. Since it is very difficult to make measurements for all values of θ and ϕ, as it would be necessary to measure the light scattered in all directions for two polarizations, the Stokes factors are used and assumptions are made that allow to measure the scattered field.

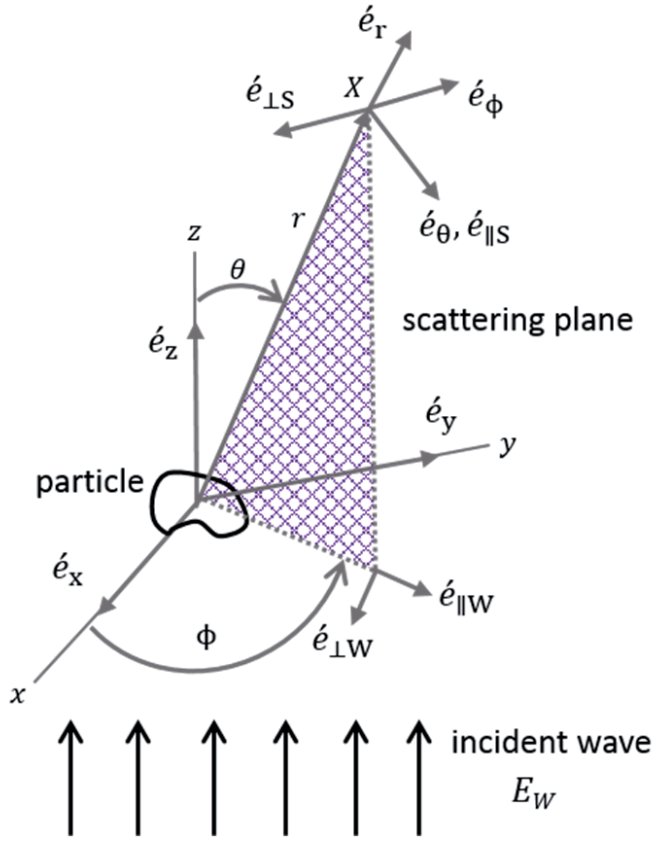

Fig. 2 Scattering at a random particle, after [7]

The elements S, S_W, S_S and S_{ext} are solutions of Poynting vectors. The electromagnetic field within the particle and its scattering can

be described by a Poynting vector. To describe the points outside the particle, equation 4, the time-averaged Poynting vector S, is used [7].

$$\vec{S} = \frac{1}{2} Re\{\vec{E}_2 \times \vec{H}_2\} = \vec{S}_W \vec{S}_S \vec{S}_{ext}$$

$$\vec{S}_W = \frac{1}{2} Re\{\vec{E}_W \times \vec{H}_W\}$$

$$\vec{S}_S = \frac{1}{2} Re\{\vec{E}_S \times \vec{H}_S\}$$

$$\vec{S}_{ext} = \frac{1}{2} Re\{\vec{E}_W \times \vec{H}_S + \vec{E}_S \times \vec{H}_W\} \quad \text{(Eq. 4)}$$

4 Mie Theory

Perhaps the most important, exactly solvable problem in particle theory is the scattering at a sphere with a random radius and refractive index. The solution to this problem has long since been derived, its practical use only became apparent with the invention of powerful computers [7]. Mie theory is a mathematical model that describes the scattering of light by particles when the particle size and wavelength of light have similar dimensions [14, 22, 34, 41, 43]. The incident plane wave and the scattered electromagnetic field are described as a series of spherical wave functions. The scattered waves are divided into three categories: the incoming wave with field $(E1, H1)$, the electromagnetic wave within the particle with field $(E2, H2)$ and the scattered wave with field $(E3, H3)$. The incoming wave is defined in polar coordinates. For the waves within the sphere and the scattered waves, the electromagnetic fields are defined with the Hertz Debey potential π. This potential is expressed by a sequential approach based on the Legendre polynomial $P_n^{(m)}(cos\,\theta)$ and the Ricatti-Bessel functions Ψ_n and X_n [34, 41, 58, 78] represented in the equation 5.

$$r\pi = \sum_{n=0}^{\infty} \sum_{m=-n}^{n} \pi_n^{(m)}$$

$$\pi_n^{(m)} = \{c_n \Psi_n(kr) + d_n \mathrm{Y}_n(kr)\} \cdot \left\{P_n^{(m)} \cdot (\cos\theta)\right\} \cdot \{a_m \cdot \cos(m\varphi) + b_m \cdot \sin(m\varphi)\} \quad \text{(Eq. 5)}$$

The coefficients a_m, b_m, c_n and d_n are scattering coefficients. In order to describe these, the Ricatti-Bessel functions are required. The Ricatti-Bessel functions are derived from the Bessel and Neumann equation $J_{(n+1/2)}$ and $N_{(n+1/2)}$. The function $h(kr)$ displays a singularity at point $kr = 0$. Only the $\Psi(kr)$ values are used to display the wave within the sphere. This is possible by a special linear combination. If $cn = 1$ and $dn = i$ the Hankel function approaches H infinitely. Both parameters can be derived from the sphere radius r, the light wavelength λ, the refractive index of the sphere $\acute{n}_1 = n_1 + ik_1$ and the refractive index n_2 of the surrounding medium [58, 78]. Thus the scattering coefficients a_m, b_m, c_n and d_n can be described. Here a_m and b_m are the coefficients for the scattering wave outside the particle, c_n and d_n are the coefficients of the wave inside the particle as shown in equation 6.

$$a_m = \frac{\Psi_n(X)\Psi'_n(mX) - m\Psi_n(mX)\Psi'_n(X)}{\xi_n(X)\Psi'_n(mX) - m\Psi_n(mX)\xi'_n(X)}$$

$$b_m = \frac{m\Psi_n(X)\Psi'_n(mX) - \Psi_n(mX)\Psi'_n(X)}{m\xi_n(X)\Psi'_n(mX) - \Psi_n(mX)\xi'_n(X)}$$

$$c_n = \frac{i}{\xi_n(X)\Psi'_n(mX) - m\Psi_n(mX)\xi'_n(X)}$$

$$d_n = \frac{i}{m\xi_n(X)\Psi'_n(mX) - \Psi_n(mX)\xi'_n(X)} \quad \text{(Eq. 6)}$$

The dashes on the functions in the equation mean partial derivations according to the argument of the respective function [7,78]. A distinction is also made between near-field and far-field scattering waves. The radial components of the scatter field decrease quadratically depending on the radius $(\alpha\, r^{-2})$, the orthogonal component decreases linearly depending on the radius $(\alpha\, r^{-1})$. Thus, the wave is recognized as purely transverse at a large distance. With this assumption it is possible to determine the scattering coefficients a_m and b_m of all measurable quantities related to the scattering and absorption of the particle, including the scattering matrix around the particle [7]. For this purpose, it is assumed that the series development of the scatter field converges. The series can be terminated after a certain number of m – terms. The error caused by the termination is very small, for all kr, if there are enough steps m. This results in $\theta = 0$ for the elements $S_{1,2}$ of the scatter matrix in forward direction with, as described in equation 7.

$$S_1(0°) = S_2(0°) = S(0°) = \frac{1}{2} \sum_n (2n+1)\,(a_m + b_m) \quad \text{(Eq. 7)}$$

Thus the scatter matrix for the consideration of the incident wave can be simplified and can be rewritten with terms for the series development to equation 8.

$$\begin{pmatrix} I_S \\ Q_S \\ U_S \\ V_S \end{pmatrix} = \frac{1}{k^2 r^2} \begin{pmatrix} S_{11} & S_{12} & 0 & 0 \\ S_{12} & S_{11} & 0 & 0 \\ 0 & 0 & S_{33} & S_{34} \\ 0 & 0 & -S_{34} & S_{33} \end{pmatrix} \begin{pmatrix} I_W \\ Q_W \\ U_W \\ V_W \end{pmatrix}$$

$$S_{11} = \frac{1}{2}(|S_2|^2 + |S_1|^2);\; S_{12} = \frac{1}{2}(|S_2|^2 - |S_1|^2);$$

$$S_{33} = \frac{1}{2}(S_2{}^* S_1 + S_2 S_1{}^*);\; S_{34} = \frac{i}{2}(S_1 S_2{}^* + S_2 S_1{}^*) \quad \text{(Eq. 8)}$$

5 Examples for the application of Mie simulations

The mathematical modelling of real systems is becoming more and more important, as it enables preliminary considerations to

be carried out cost-effectively and relatively simply. In this review the simulation program MiePlot is used [53]. The scattering depends on the incident light wave, the refractive index of the scattering medium and the surrounding system, the scattering angle and the particle size. For the simulation, this means that all but one of these variables are kept constant and one is varied within a specified range. The program performs numerical simulation calculations according to Mie theory, based on the explanations of Bohr and Huffmann [7]. This will be illustrated by two particle types: monodisperse, spherical polystyrene particles and precipitated wheat protein particles. The exact description of the simulation and the measurement procedure can be found here [73]. The backscatter pattern for polychrome light is examined. The scattering angle remains constant. For the simulation of the particles backscattering is assumed in an angle range of 170° to 180°. Figure 3 shows the result for this observation case for two particle sizes for illustration with measured values of polystyrene recorded in backscattering. The number of peaks increases with increasing particle size. The illustration shows that the distinct frequencies of polychrome light are scattered differently which demonstrates the principle behind elastic, static light scattering. Elastic implies the scattered light is diffracted differently depending on the wavelength and the particle size, however there is no excitation or emission at the scattering medium. These changes in the diffraction can be measured by SLS – probe.

Even if Mie theory has ideal spheres as a basis for calculation, it can also be used to measure particles that are not entirely spherical. Protein particles are not quite round in shape, they are slightly elliptical, but it is also possible to compare the measurements with simulations, as shown in figure 4. The generation of these wheat protein particles is described elsewhere [73].

In order to be able to carry out the later prediction of the particle size, a refractive index-dependent database must be created, i.e. the refractive index of the particles to be measured must be known. Figure 5 shows an example of such a recursion of the measured data compared to the simulated data, in addition to the trace and linear reconstruction of the least squares.

The individual curves that contribute to the linear reconstruction are visualized. In addition,

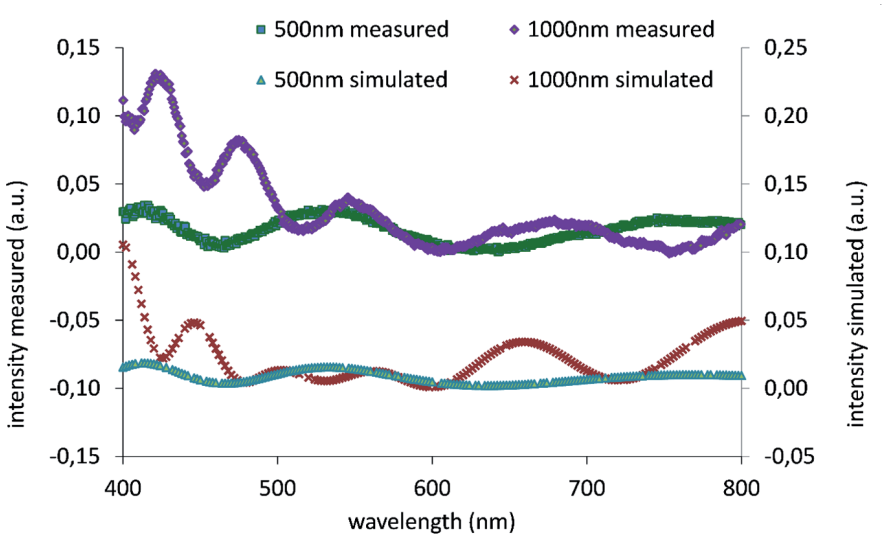

Fig. 3 **Simulated and measured backscatter pattern of polystyrene particles. Diameter of the particles 500 nm and 1000 nm, according to [73]**

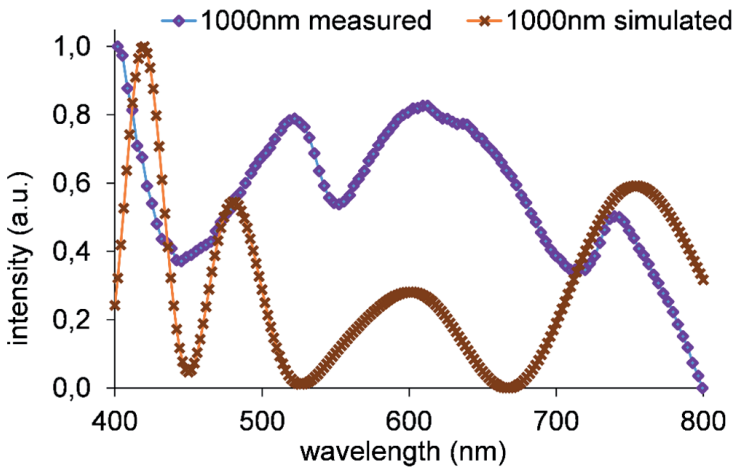

Fig. 4 **Simulated and measured backscatter pattern of wheat proteins according to [73]**

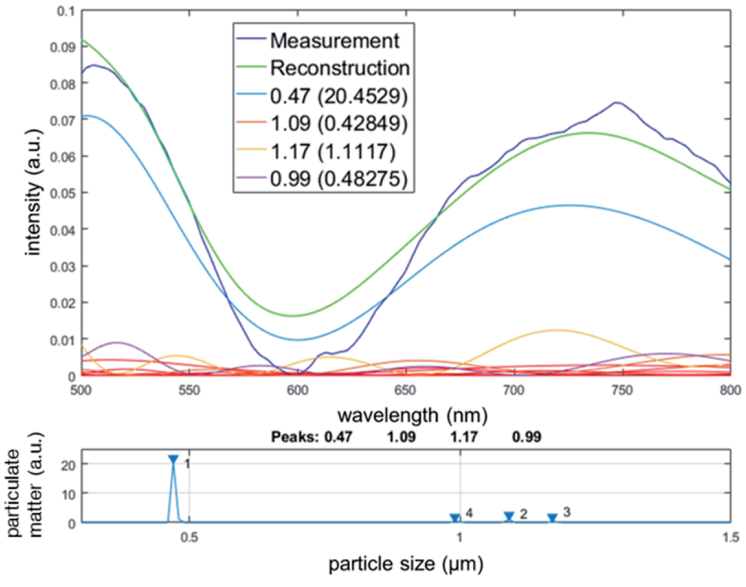

Fig. 5 **Recursion of measured monodisperse polystyrene particles, with diameter 0.5 µm, measured in backscatter based on Mie scattering [73]**

a histogram can be seen showing the particle size determined in the reconstruction. In this histogram, which is located at the bottom of figure 5, the particle sizes determined on the basis of recursion are displayed. The peak value 0.47 indicates that the measured curve has its closest match with the curve for a diameter of 0.47 µm from the simulation database. The values 1.09, 1.17, and 0.99 are also given as possible particle diameters, but can be excluded due to their very insignificant participation in the prediction. Although the peaks are slightly shifted, the number of peaks is similar and their simulated and analysed wavelengths correlate. A recursion can be used to determine the match. The recursion shows the repetition of the measurement curve with the simulated curve. For this purpose, the measured data is processed and compared on the basis of a recursion with a previously created scatter curve database based on Mie theory.

6 Conclusion

With the ability to measure and simulate particles, it is possible to perform recursions. For this purpose, the measured data are approximated in the form of a mathematical treatment. The approximation of a measurement curve describes the procedure for regression of a function curve to a data field. Different models can be applied depending on the type of data field. In order to increase the quality of the fit, a model is first selected that best describes the data field, such as a linear, polynomial or sinusoidal model. These models can be expressed by general function equations. The aim of the approximation is to determine the coefficients so that the deviation from the measured data points is minimal. A frequently used method is the least squares method. To quantify the quality of the fit, the Mean Squared Error (MSE) can be calculated. The smaller the MSE, the better the quality of the fit. Since an absolute value is formed here, it cannot be compared with the MSE of the approximation of another data set. Boundary conditions could be added that require the solution to be a specially ordered set. If no similarity is detected here, the process will not run as desired. Similarly, multimodal systems can be described by changing the boundary conditions by combining learning algorithms. The limitation for such particle size measurements lies in the physics behind the Mie theory in combination with the test setup used. Currently only particles between 200 nm and 1000 nm can be measured. To measure particles out of this range, the associated mathematical models and theories for these size ranges must be stored and correlated in the program matrix. The particle size distribution in combination with the particle concentration, however, provides sufficient information for rapid monitoring of changes in overall quality. The small and simple design of the probe head allows easy integration into different process environments, e.g. into a continuous wort flow after the lauter stage. In addition, high pressures, high temperatures up to 180 °C or other CIP conditions do not affect the functionality of the probe head. The coupling of the sensor head to the electronic assembly by means of glass fibres separates the dry and wet areas of the device. The set-up described should now be tested in brewing environments in real time. Scattering measurement could also be used as a process tool for intermediate control of beer quality during filtration of the entire beer production process to monitor beer quality.

This paper explains the physical theoretical basis of the SLS and points out the potential for particle scattering measurements during the production of beer. With this approach different possibilities can be explored in order to develop inline or online backscattering systems for particle size analysis in liquid systems. This allows continuous monitoring of particle size as well as local and temporal concentration. In combination with other measured variables, such as temperature, pH value, oxygen concentration, etc., the measurement method presented here can help to monitor and control the brewing process.

7 References

1. Arias, M. L. and Frontini, G. L.: Particle Size Distribution Retrieval from Elastic Light Scattering Measurements by a Modified Regularization Method, Particle & Particle Systems Characterization, **23** (2006), no. 5, pp. 374-380.
2. Arndt, K.-F.; Witkowski, K. and Schimmel, K.-H.: Quasielastische Lichtstreuung von gequollenen Siliconnetzwerken, Acta Polymerica, **39** (1988), no. 9, pp. 475-479.
3. Aron, P. M. and Shellhammer, T. H.: A Discussion of Polyphenols in Beer Physical and Flavour Stability, Journal of the Institute of Brewing, **116** (2010), no. 4, pp. 369-380.
4. Bamforth, C. W.: 125th Anniversary Review: The Non-Biological Instability of Beer, Journal of the Institute of Brewing, **117** (2011), no. 4, pp. 488-497.
5. Barth, H. G. and Flippen, R. B.: Particle Size Analysis, Analytical Chemistry, **67** (1995), no. 12, pp. 257-272.
6. Baxter, N. J.; Lilley, T. H.; Haslam, E. and Williamson, M. P.: Multiple Interactions between Polyphenols and a Salivary Proline-Rich Protein Repeat Result in Complexation and Precipitation †, Biochemistry, **36** (1997), no. 18, pp. 5566-5577.
7. Bohren, C. F. and Huffman, D. R.: Absorption and scattering of light by small particles, Wiley-VCH, Weinheim, 2004.
8. Braun, F.; Hildebrand, N.; Wilkinson, S.; Back, W.; Krottenthaler, M. and Becker, T.: Large-Scale Study on Beer Filtration with Combined Filter Aid Additions to Cellulose Fibres, Journal of the Institute of Brewing, **117** (2011), no. 3, pp. 314-328.
9. Cai, G.; Li, X.; Zhang, C.; Zhang, M. and Lu, J.: Dextrin as the main turbidity components in wort produced from major malting barley cultivars of Jiangsu province in China: Dextrin, the main component of Dan'er wort turbid, Journal of the Institute of Brewing, **122** (2016), no. 3, pp. 543-546.
10. Carrasco, A. and Siebert, K. J.: Human visual perception of haze and relationships with instrumental measurements of turbidity. Thresholds, magnitude estimation and sensory descriptive analysis of haze in model systems, Food Quality and Preference, **10** (1999), no. 6, pp. 421-436.
11. Chapon, L.: The mineral composition of chill haze preparations, Journal of the Institute of Brewing, **71** (1965), no. 4, pp. 299-304.
12. Chapon, L.: Nephelometry as a method for studying the relations between polyphenols and proteins, Journal of the Institute of Brewing, **99** (1993), no. 1, pp. 49-56.
13. Cole, G. J.: Haze in E.B.C. worts, Journal of the Institute of Brewing, **69** (1963), no. 4, pp. 338-342.
14. Debye, P.: Light Scattering in Solutions, Journal of Applied Physics, **15** (1944), no. 4, pp. 338–342.
15. Delvaux, F.; Delvaux, F. R. and Delcour, J. A.: Characterisation of the Colloidal Haze in Commercial and Pilot Scale Belgian White Beers,

Journal of the Institute of Brewing, **106** (2000), no. 4, pp. 221-228.
16. Elumalai, R.; Sridhar, P.; Malmurugan, N. and Nagappan: Computer based off line haze meter to measure beer haze and to determine the purity of beer, 2000, pp. 616-620.
17. Gabriel, P.; Sladký, P. and Sigler, K.: A new rapid high-throughput method for prediction of beer colloidal stability: Method for prediction of beer colloidal stability, Journal of the Institute of Brewing, **122** (2016), no. 2, pp. 304-309.
18. Grasser, A. and Woest, V.: Chemie des Bieres, Chemkon, **16** (2009), no. 3, pp. 125-131.
19. Gulari, E.; Bazzi, G.; Gulari, E. and Annapragada, A.: Latex Particle Size Distributions from Multiwavelength Turbidity Spectra, Particle & Particle Systems Characterization, **4** (1987), no. 1-4, pp. 96-100.
20. Hartmann, K.: Bedeutung rohstoffbedingter Inhaltsstoffe und produktionstechnologischer Einflüsse auf die Trübungsproblematik im Bier, Technische Universität München, 2006, Retrieved February 4, 2019 from http://nbn-resolving.de/urn/resolver.pl?urn:nbn:de:bvb:91-diss20061204-1415087272.
21. Hofmann, T.: Kolloide: Die Welt der vernachlässigten Dimensionen, Chemie in unserer Zeit, **38** (2004), no. 1, pp. 24-35.
22. Horvath, H.: Gustav Mie and the scattering and absorption of light by particles: Historic developments and basics, Journal of Quantitative Spectroscopy and Radiative Transfer, **110** (2009), no. 11, pp. 787-799.
23. Hudson, J. R.: Metals in beer haze, Journal of the Institute of Brewing, **64** (1958), no. 2, pp. 157-161.
24. Izawa, M.; Takashio, M. and Tamaki, T.: Determination of high molecular weight β-glucan in wort and beer using a post-column calcofluor flow-injection-analysis (FIA) method, Journal of the Institute of Brewing, **102** (1996), no. 3, pp. 183-189.
25. Jin, B.; Li, L.; Feng, Z.-C.; Li, B.; Liu, G.-Q. and Zhu, Y.-K.: Investigation of hordeins during brewing and their influence on beer haze by proteome analysis: hordein during brewing and their influence on beer haze, Journal of Food Biochemistry, **35** (2011), no. 5, pp. 1522-1527.
26. Juvonen R. and Haikara, A.: Amplification Facilitators and Pre-Processing Methods for PCR Detection of Strictly Anaerobic Beer-Spoilage Bacteria of the Class Clostridia in Brewery Samples, Journal of the Institute of Brewing, **115** (2009), no. 3, pp. 167-176.
27. Kanauchi, M.; Ishikura, W. and Bamforth, C. W.: β-Glucans and Pentosans and their Degradation Products in Commercial Beers, Journal of the Institute of Brewing, **117** (2011), no. 1, pp. 120-124.
28. Kanauchi, M.; Milet, J. and Bamforth, C. W.: Oxalate and Oxalate Oxidase in Malt, Journal of the Institute of Brewing, **115** (2009), no. 3, pp. 232-237.
29. Kätzel, U.; Stintz, M. and Ripperger, S.: Applikationsuntersuchungen zur Photonenkorrelationsspektroskopie im Rückstreubereich, Chemie Ingenieur Technik, **76** (2004), no. 12, pp. 66-69.
30. Kunze, W. and Manger, H.-J.: Technologie Brauer & Mälzer, VLB, Berlin, 2011.
31. Kusche, M.: Kolloidale Trübung in untergärigen Bieren, Technische Universität München, 2005, Retrieved from http://nbn-resolving.de/urn/resolver.pl?urn:nbn:de:bvb:91-diss20050822-1753220312
32. Lehner, G.: Elektromagnetische Feldtheorie: für Ingenieure und Physiker, Springer Vieweg, Berlin, 2018.
33. Leschonski, K.: Die On-Line-Messung von Partikelgrößenverteilungen in Gasen und Flüssigkeiten, Chemie Ingenieur Technik, **50** (1978), no. 3, pp. 194-203.
34. Lorenz, L.: Ueber die Refractionsconstante, Annalen der Physik und Chemie, **247** (1880), no. 9, pp. 70-103.
35. Masár, M.; Žúborová, M.; Kaniansky, D. and Stanislawski, B.: Determination of oxalate in beer by zone electrophoresis on a chip with conductivity detection, Journal of Separation Science, **26** (2003), no. 8, pp. 647-652.
36. Maxwell, J. C.: VIII. A dynamical theory of the electromagnetic field, Philosophical Transactions of the Royal Society of London, 1865, no. 155, pp. 459-512.
37. McClements, D. J.; Chantrapornchai, W. and Clydesdale, F.: Prediction of Food Emulsion Color Using Light Scattering Theory, Journal of Food Science, **63** (2006), no. 6, pp. 935-939.
38. McMurrough, I. and Baert, T.: Identification of proanthocyanidins in beer and their direct measurement with a dual electrode electrochemical detector, Journal of the Institute of Brewing, **100** (1994), no. 6, pp. 409-416.
39. van der Meeren, P.; Bogaert, H.; Vanderdeelen, J. and Baert, L.: Relevance of Light Scattering Theory in Photon correlation spectroscopic experiments, Particle & Particle Systems Characterization, **9** (1992), no. 1-4, pp. 138-143.
40. Meredith W. O. S. and Tkachuk, R.: Chill haze protein of barley, malt and beer, Journal of the Institute of Brewing, **70** (1964), no. 5, pp. 410-415.
41. Mie, G.: Beiträge zur Optik trüber Medien, speziell kolloidaler Metallösungen, Annalen der Physik, **330** (1908), no. 3, pp. 377-445.
42. Miedaner, H. and Mitteleuropäische Brautechnische Analysenkommission (eds.): Brautechnische Analysenmethoden: Methodensammlung der Mitteleuropäischen Brautechnischen Analysenkommission (MEBAK), Bd. 2: ... Selbstverl. der MEBAK, Freising-Weihenstephan, 2002.
43. Mishchenko, M. I.: Gustav Mie and the fundamental concept of electromagnetic scattering by particles: A perspective, Journal of Quantitative Spectroscopy and Radiative Transfer, **110** (2009), no. 14-16, pp. 1210-1222.
44. Mitchell, A. E.; Hong, Y.-J.; May, J. C.; Wright, C. A. and Bamforth, C. W.: A Comparison of Polyvinylpolypyrrolidone (PVPP), Silica Xerogel and a Polyvinylpyrrolidone (PVP)-Silica Co-Product for Their Ability to Remove Polyphenols from Beer, Journal of the Institute of Brewing, **111** (2005), no. 1, pp. 20-25.
45. Morris, T. M.: Particle size analysis of beer solids using a coulter counter, Journal of the Institute of Brewing, **90** (1984), no. 3, pp. 162-166.
46. Morris, T. M.: The relationship between haze and the size of particles in beer, Journal of the Institute of Brewing, **93** (1987), no. 1, pp. 13-17.
47. Munck, L.; Jorgensen, K. G.; Ruud-Hansen, J. and Hansen, K. T.: The ebc methods for determination of high molecular weight β-glucan in barley, malt, wort and beer, Journal of the Institute of Brewing, **95** (1989), no. 2, pp. 79-82.
48. Mundy, A. P. and Boley, N..: A Survey of Instrumentation used for the Determination of Haze in Beer, Journal of the Institute of Brewing, **105** (1999), no. 2, pp. 75-78.
49. Mussche R. A. and Pauw, C.: Total Stabilisation of Beer in a Single Operation*, Journal of the Institute of Brewing, **105** (1999), no. 6, pp. 386-391.
50. Narziß, L.; Back, W.; Gastl, M. and Zarnkow, M.: Abriss der Bierbrauerei, Wiley-VCH Verlag GmbH & Co. KGaA, Weinheim, 2017.
51. Papp, A.; Winnewisser, W.; Geiger, E. and Briem, F.: Influence of (+)-Catechin and Ferulic Acid on Formation of Beer Haze and Their Removal through different Polyvinylpolypyrollidone-Types, Journal of the Institute of Brewing, **107** (2001), no. 1, pp. 55-60.
52. Perretti, G.; Floridi, S.; Turchetti, B.; Marconi, O. and Fantozzi, P.: Quality Control of Malt: Turbidity Problems of Standard Worts Given by the Presence of Microbial Cells, Journal of the Institute of Brewing, **117** (2011), no. 2, pp. 212-216.

53. Laven, P.: MiePlot. Retrieved from http://www.philiplaven.com/mieplot.htm#Download%20MiePlot
54. Poncetlegrand, C.; Edelmann, A.; Putaux, J.; Cartalade, D.; Sarnimanchado, P. and Vernhet, A.: Poly(l-proline) interactions with flavan-3-ols units: Influence of the molecular structure and the polyphenol/protein ratio, Food Hydrocolloids, **20** (2006), no. 5, pp. 687-697.
55. Poncet-Legrand, C.; Cartalade, D.; Putaux, J.-L.; Cheynier, V. and Vernhet, A.: Flavan-3-ol Aggregation in Model Ethanolic Solutions: Incidence of Polyphenol Structure, Concentration, Ethanol Content, and Ionic Strength, Langmuir, **19** (2003), no. 25, pp. 10563-10572.
56. Poncet-Legrand, C.; Gautier, C.; Cheynier, V. and Imberty, A.: Interactions between Flavan-3-ols and Poly(L -proline) Studied by Isothermal Titration Calorimetry: Effect of the Tannin Structure, Journal of Agricultural and Food Chemistry, **55** (2007), no. 22, pp. 9235-9240.
57. Puskas, J. E.; Foreman, E. A.; Dos Santos, L. M. and Soytaş, S. H.: Characterization of Polymer Architectures by Multidetection Size Exclusion Chromatography, Macromolecular Symposia, **261** (2008), no. 1, pp. 85-90.
58. Ray, A. K.; Souyri, A.; Davis, E. J. and Allen, T. M.: Precision of light scattering techniques for measuring optical parameters of microspheres, Applied Optics, **30** (1991), no. 27, pp. 3974.
59. Reed, R. J. R.: Centenary Review Article Beer Filtration, Journal of the Institute of Brewing, **92** (1986), no. 5, pp. 413-419.
60. Rice, C. J.; Pawlowsky, K. and Smart, C.: Evaluating haze formation in flavoured lager beers using a range of forcing methods: Evaluating haze formation in flavoured lager beers, Journal of the Institute of Brewing, **123** (2017), no. 3, pp. 388-395.
61. Roy, D. and Fendler, J.: Reflection and Absorption Techniques for Optical Characterization of Chemically Assembled Nanomaterials, Advanced Materials, **16** (2004), no. 6, pp. 479-508.
62. Satinover, S. J.; Dove, J. D. and Borden, M. A.: Single-Particle Optical Sizing of Microbubbles, Ultrasound in Medicine & Biology, **40** (2014), no. 1, pp. 138-147.
63. Savage, D. J. and Thompson, C. C.: Electrofocusing studies on the formation of beer haze, Journal of the Institute of Brewing, **78** (1972), no. 6, pp. 472-476.
64. Sensidoni, M.; Marconi, O.; Perretti, G.; Freeman, G. and Fantozzi, P.: Monitoring of Beer Filtration Using Photon Correlation Spectroscopy (PCS), Journal of the Institute of Brewing, **117** (2011), no. 4, pp. 639-646.
65. Siebert, K. J.: Haze formation in beverages, LWT – Food Science and Technology, **39** (2006), no. 9, pp. 987-994.
66. Siebert, K. J. and Lynn, P. Y.: Haze-Active Protein and Polyphenols in Apple Juice Assessed by Turbidimetry, Journal of Food Science, **62** (1997), no. 1, pp. 79-84.
67. Speers, R. A.; Jin, Y.-L.; Paulson, A. T. and Stewart, R. J.: Effects of β-Glucan, Shearing and Environmental Factors on the Turbidity of Wort and Beer, Journal of the Institute of Brewing, **109** (2003), no. 3, pp. 236-244.
68. Steiner, E.; Becker, T. and Gastl, M.: Turbidity and Haze Formation in Beer – Insights and Overview, Journal of the Institute of Brewing, **116** (2010), no. 4, pp. 360-368.
69. Steiner, E.; Gastl, M. and Becker, T.: Protein changes during malting and brewing with focus on haze and foam formation: a review, European Food Research and Technology, **232** (2011), no. 2, pp. 191-204.
70. Steinke, L.; Wessely, B. and Ripperger, S.: Optische Extinktionsmessverfahren zur Inline-Kontrolle disperser Stoffsysteme, Chemie Ingenieur Technik, **81** (2009), no. 6, pp. 735-747.
71. Stewart, D.; Freeman, G. and Evans, E.: Development and Assessment of a Small-Scale Wort Filtration Test for the Prediction of Beer Filtration Efficiency, Journal of the Institute of Brewing, **106** (2000), no. 6, pp. 361-366.
72. Surbek, M.; Esen, C.; Schweiger, G. and Ostendorf, A.: Pollen characterization and identification by elastically scattered light, Journal of Biophotonics, **4** (2011), no. 1-2, pp. 49-56.
73. Teumer, T.; Capitain,C.; Ross-Jones, J.; Tippkötter, N.; Rädle, M. and Methner, F.-J.: In-line Haze Monitoring Using a Spectrally Resolved Back Scattering Sensor, BrewingScience, **71** (2018), no. 5-6, pp. 49-55.
74. Teumer, T.; Hufnagel, T.; Schäfer, T.; Schlarp-Horvath, R.; Karbstein, H. P.; Methner, F.-J. and Rädle, M.: Entwicklung eines Partikelmesssystems zur Erfassung geringer Streulicht-Intensitäten optimiert für den Einsatz sehr schwacher Laserstrahlen, Chemie Ingenieur Technik, **91** (2018), no. 4, pp. 529-533.
75. Tüzün, U. and Farhadpour, F. A.: Comparison of Light Scattering with other Techniques for Particle Size Measurement, Particle & Particle Systems Characterization, **2** (1985), no. 1-4, pp. 104-112.
76. Urban, D. and Takamura, K. (eds.): Polymer dispersions and their industrial applications, Wiley-VCH, Weinheim, 2002.
77. Vega, J. R.; Frontini, G. L.; Gugliotta, L. M. and Eliçabe, G. E.: Particle Size Distribution by Combined Elastic Light Scattering and Turbidity Measurements, A Novel Method to Estimate the Required Normalization Factor, Particle & Particle Systems Characterization, **20** (2003), no. 6, pp. 361-369.
78. Vortisch, H.: Beobachtung von Phasenübergängen in einzeln levitierten Schwefelsäuretröpfchen mittels Raman-Spectroskopie und elastischer Lichtstreuung, FU Berlin, Berlin, 2002, Retrieved March 5, 2019 from http://webdoc.sub.gwdg.de/ebook/diss/2003/fu-berlin/2002/299/index.html
79. Ye, L.; Huang, Y.; Li, M.; Li, C. and Zhang, G.: The chemical components in malt associated with haze formation in beer: Chemical components in malt, Journal of the Institute of Brewing, **122** (2016), no. 3, pp. 524-529.
80. Ziegler, A.; Schock-Kusch, D.; Kapoustina, V.; Braun, F.; Dounia, S.; Stahl, U. and Rädle, M.: Einfluss des Nährmediums auf die Bewegungscharakteristik von *Bacillus amyloliquefaciens*, Chemie Ingenieur Technik, **88** (2016), no. 6, pp. 809-817.
81. Zinth, W. and Aumüller, U.: Optik: Lichtstrahlen – Wellen – Photonen, Oldenbourg, München, 2009.
82. Lagaly, G.; Schulz, O.; Zimehl, R.: Dispersionen und Emulsionen – Eine Einführung in die Kolloidik feinverteilter Stoffe einschließlich der Tonminerale, Steinkopff, Heidelberg, 1997, Retrieved January 31, 2019 from http://nbn-resolving.de/urn:nbn:de:1111-201109214107
83. Batchvarov, V. and Kellner, V.: Determination of Alcohol Chill Haze in Beer, Journal of the Institute of Brewing, **110** (2004), no. 3, pp. 240-241.

Received 11 June 2019, accepted 7 August 2019